Journal of Engineering Science *Vol. XXX, no. 4 (2023), pp. 8 - 19*
Fascicle *Industrial Engineering* *ISSN 2587-3474*
Topic *Mechanical Engineering and Technologies* *eISSN 2587-3482*

https://doi.org/10.52326/jes.utm.2023.30(4).01
UDC 621.671:004.9

EMPIRICAL MODELS' APPLICABILITY FOR CALCULATING THE CENTRIFUGAL PUMP'S IMPELLERS GEOMETRIC PARAMETERS

Viorel Bostan[1], ORCID: 0000-0002-2422-3538,
Andrei Petco[1,2*], ORCID: 0009-0004-0577-3296,
Ion Șaragov[1], ORCID: 0009-0001-5701-6885

[1] *Technical University of Moldova, 168 Stefan cel Mare Blvd., Chisinau, Republic of Moldova*
[2] *S.R.L. "CRIS" 68/2-69 Albisoara str., Chisinau, Republic of Moldova*
*Corresponding author: Andrei Petco, *andrei.petco@tcm.utm.md*

Received: 10. 19. 2023
Accepted: 11. 24. 2023

Abstract. This paper deals with the comparison of empirical computational models used to achieve the geometrical parameters of pumps impellers with models based on Computational Fluid Dynamics (CFD) simulations and optimization algorithms. Also, the actuality of the empirical models application in modern pump manufacturing industry is analyzed. Further, an empirical model for calculating the pump impeller geometrical parameters was presented. Applying this model, the calculation of the centrifugal pump impeller parameters for CH 6,3/20 1,1-2 canned motor pump was performed. The procedure for parameterization and generation of the geometric model based on parameters obtained from this model through ANSYS DesignModeler was also presented. CFD simulation based on ANSYS CFX was used to obtain the operating characteristic of the obtained centrifugal pump impeller. The authors carried out the comparison of the results of the designed model with the original one and with the optimized impeller obtained using optimization algorithms and CFD calculations.

Keywords: *pump impeller, centrifugal pumps, analytical calculation, CFD simulations.*

Rezumat. În această lucrare este prezentată compararea modelelor de calcul empirice utilizate pentru realizarea parametrilor geometrici ai rotoarelor pompelor cu modele bazate pe simulări CFD și algoritmi de optimizare. De asemenea, este analizată actualitatea aplicării modelelor empirice în industria modernă de fabricare a pompelor. Totodată, a fost prezentat un model empiric pentru calcularea parametrilor geometrici ai rotorului pompei. Aplicând acest model, s-a efectuat calculul parametrilor rotorului pompei centrifuge pentru pompă centrifugă cu motor capsulat CH 6,3/20 1,1-2. A fost prezentată procedura de parametrizare și generare a modelului geometric pe baza parametrilor obținuți din acest model prin intermediul ANSYS DesignModeler. Simularea CFD bazată pe ANSYS CFX a fost utilizată pentru a obține caracteristicele de funcționare a rotorului pompei centrifuge. Rezultatele modelului proiectat au fost comparate cu cel original și cu rotorul optimizat obținut folosind algoritmi de optimizare și calcule CFD.

Cuvinte cheie: *rotorul pompei, pompe centrifuge, calcul analitic, simulări CFD.*

1. Introduction

Obtaining the geometry of turbomachines impellers is a complex problem, which can be solved in several ways: the application of empirical models [1], based on experimentally obtained data; specialized software that automates previous models [2,3]; and optimizations based on Computational Fluid Dynamics (CFD) simulations and optimization algorithms [4–7].

The paper presents the application of an empirical model to obtain a rotor with enhanced characteristics.

Since the beginning of the 20th century, due to more determination of the parameters of fluid flow in the working parts of centrifugal pumps, empirical models for calculating the working parts of centrifugal pumps have obtained their contemporary form. To obtain the geometry of the pump parts, design engineers made use of the empirical mathematical models presented in the works of Pfleiderer (Germany, 1924), Stepanoff (USA, 1948), Lomakin (USSR, 1950) etc.

Before the massive application of CFD simulations, the design of pump working parts was reduced to a large number of experimental iterations [8], with the geometry of the pump parts changing at each optimization stage. In this paper, the optimized impeller received by applying CFD simulations together with optimization algorithms [9], was compared with the impeller obtained using analytical methods (primarily based on the model evolution presented in the work [10]).

2. Theoretical considerations about centrifugal pump efficiency

The authors selected the centrifugal pump efficiency as the investigated criterion. The Pump efficiency η represents the ratio of useful power P_u and delivered power P and can be represented by the following relation [11]:

$$\eta = \frac{P_u}{P} = \frac{\rho g Q H}{P}, \tag{1}$$

where: P is the total power,

P_u – used power,

Q – fluid flow rate measured at the discharge pump connection,

H – pump head.

The losses in the centrifugal pump, in case of a centrifugal pump with a canned motor (Figure 1) in its pumping part, are divided into hydraulic, volumetric, and mechanical losses. The efficiency of the pumping part is calculated by Eq. (2) [8, 12–15]:

$$\eta_{p.m.} = \eta_m \eta_h \eta_v, \tag{2}$$

where*:* η_h is the hydraulic efficiency, η_v is the volumetric efficiency, and η_m is the mechanical efficiency.

Hydraulic efficiency η_h of a centrifugal pump indicates the efficiency a pump converts the mechanical energy supplied by the electric motor into the hydraulic energy of the pumped fluid [8, 10–12,16–19]:

$$\eta_h = \frac{H_t - \Sigma h}{H_t}, \tag{3}$$

where: H_t is the theoretical pump head, and Σh is the sum of the hydraulic losses.

The following logarithmic relation is given for the preventive determination of the hydraulic efficiency η_h [5]:

$$\eta_h = 0{,}7 + 0{,}0835 lg D_q, \quad (4)$$

where: parameter $D_q = 4\sqrt[3]{\frac{Q}{n}}$ is the nominal diameter, *n* being the pump shaft speed.

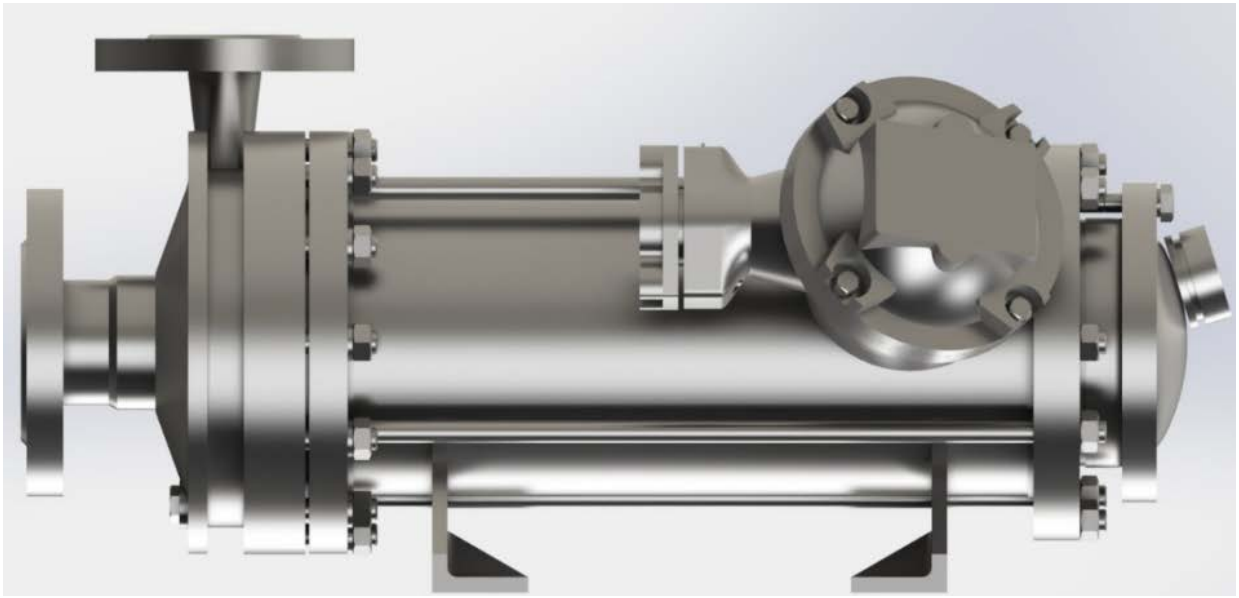

Figure 1. Representation of the pump model CH 6,3/20 1,1-2.

Hydraulic losses. The first type of energy loss in a pump is the one caused by the hydraulic resistance to flow movement in the working parts of the pump being exceeded [17]. By the friction losses during fluid movement in the channels of the flowing part of the pump and losses due to the formation of vortices associated with the separation of the fluid when flowing around different elements of the working parts of the pump [11].

Hydraulic losses occur due to frictional forces within the fluid, formation of areas of increased turbulence, variation of flow direction, variation of the area and cross-sectional shape of the pump part channels and losses caused due to flow separation from the impeller walls.

The volumetric efficiency η_v of a centrifugal pump points out the efficiency of conveying the fluid flow. It is equal to the ratio of the pump's actual flow rate *Q* to the ideal flow rate Q_i [8,10–12, 16–19]:

$$\eta_v = \frac{Q}{Q_i} = \frac{Q}{Q+Q_P}, \quad (5)$$

where*:* Q_i is the total flow and Q_p is the lost flow.

For achieving the preventive determination of volumetric efficiency η_v the following relation was used [10,11,18]:

$$\eta_v = \frac{1}{1+0{,}68 \cdot n_s^{-\frac{2}{3}}}. \quad (6)$$

Volume losses occur in the gaps between rotating and stationary parts, where fluid leaks occur, reducing pump flow. Volume losses in the pump are often related to the liquid flow from the impeller's discharge area to its suction area. In order to minimize the leakage flow due to pressure differences, the fit between the impeller and the pump casing is reduced to a maximum [11,18].

Mechanical efficiency η_m of the centrifugal pump is the ratio of the power delivered by the motor to the useful mechanical power of the pump [8,10–12,16–19]:

$$\eta_m = \frac{P_M - \Delta P}{P_M} = 1 - \frac{\Delta P}{P_M}. \quad (7)$$

The following relation is used in the preventive determination of the mechanical efficiency η_m [11]:

$$\eta_m = \frac{1}{1+\frac{820}{n_S{}^2}}. \quad (8)$$

Mechanical losses are due to friction of the bearings, shaft seals and friction of the outer surface of the impellers with the liquid (friction of the hub and shroud disks) [16,17]. Mechanical losses are divided into internal and external losses [11].

The external mechanical losses depend on the shaft dimensions, the type of end seals and the rotational speed of the impeller and are attested in seals, slide bearings and journals. Internal mechanical losses represent the losses occurred through hydraulic friction of the hub and shroud disks.

For centrifugal canned motor CH and CMP type pumps, where the pumping part and the electric motor are joined by a shaft, the total efficiency of the pump represents the result of multiplying of the efficiencies of the pumping part and the electric motor:

$$\eta = \eta_{p.m.} \cdot \eta_{m.e.} = \eta_m \eta_h \eta_v \cdot \eta_{m.m.} \eta_{e.m.}, \quad (9)$$

where: $\eta_{m.m.}$ is the mechanical efficiency of the electric motor,

$\eta_{e.m.}$ is the electromagnetic efficiency of the pump's electric motor.

We can mention that during the study the pump's electric motor has not been modified, its efficiency remained constant ($\eta_{m.m.} = \eta_{e.m.} = const$). As the mechanical and volumetric efficiency of the pump impeller did not change considerably, it can also be considered constant ($\eta_m = \eta_v = const$), therefore in the given case, the study of the variation on the pump impeller hydraulic efficiency is of interest η_h.

3. Modelling the geometry of the centrifugal pump impeller

The empirical model described in [10,11,16–19], was used to obtain the parameters of the geometrical model of the pump impeller. We can mention the main relations of calculation of the centrifugal pump impeller parameters:

First, we determine the type of pump according to the corresponding specific speed [11,18]:

$$n_s = \frac{3{,}65 \cdot n\sqrt{Q}}{H^{\frac{3}{4}}}, \quad (10)$$

where: *n* is the impeller rotational frequency, *Q* is the pump flow rate at the pump outlet, and *H* is the pumping head.

To determine the dimensions of the impeller hub, we need to determine the shaft dimensions, taking into account the pump power [10,11,18]:

$$P = \frac{\rho g Q H}{\eta}.$$

The shaft diameter is calculated [10,11,18] with the following relation:

$$d = 170\sqrt[3]{\frac{P}{\pi \tau_{cr}}}., \quad (11)$$

where: P is pump power and τ_{cr} - permissible mechanical stress at twisting.

Diameter of the impeller bushing is determined by relation [10,11,18]:

$$d_n = d(1{,}25 \div 1{,}5). \tag{12}$$

The inlet speed of the centrifugal pump is determined by the following relation:

$$v_0 \approx 0{,}06\sqrt[3]{Qn^2}.$$

The impeller's inlet diameter D_0 is calculated from the relation presented below, resulting from the fluid flow continuity equation [11]:

$$D_0 = \sqrt{\frac{4Q}{\pi\eta_v v_0} + d^2}, \tag{13}$$

where: $v_0 \approx 0{,}06\sqrt[3]{Qn^2}$ is the speed value at the inlet to the centrifugal pump.

The diameter of the blade's leading edge is established as follows:

$$D_1 = D_0 + (2 + 10)mm. \tag{14}$$

The transport speed at the impeller's blade inlet is set:

$$u_1 = \frac{\pi D_1 n}{60}. \tag{15}$$

The absolute velocity at the leading edge of the blade is calculated as below:

$$v_1 = \frac{v_0}{\psi_1}, \tag{16}$$

where: ψ_1 is the coefficient of contraction of the liquid stream by the blade.

The width of the blade at the impeller inlet is taken:

$$b_1 = 1 - \frac{Q}{\pi D_1 v_1}. \tag{17}$$

The angle of the blade is set as follows:

$$\beta_1 = arctg\frac{v_{1r}}{u_1}. \tag{18}$$

The angle obtained is increased by angle of attack $\Delta\beta_1 = 3 \div 8°$.

Constructive angle β_{1l} is determined by the following relation:

$$\beta_{1l} = \beta_1 + \Delta\beta_1,$$

where: $\Delta\beta_1 = 3 \div 8°$ is the angle of attack.

The impeller diameter is determined by the following relation:

$$D_2 = \frac{60u_2}{\pi n}, \tag{19}$$

where $u_2 = K_{u_2}\sqrt{2gH_t}$, velocity u_2 at impeller outlet.

According to Pfleiderer's relation the number of blades Z is determined as follows:

$$Z = 6{,}5\frac{D_2 + D_1}{D_2 - D_1} sin\left(\frac{\beta`_2 - \beta`_1}{2}\right), \tag{20}$$

where: in the first approximation [10,18]: $\beta`_1 = \beta_1 = 15 \div 30°$ and $\beta`_2 = \beta_2 = 18 \div 20°$.

The number of blades received is rounded up to a whole number.

The analytical calculation of the geometrical parameters of the pump CH 6,3/20 1,1-2 impeller (Figure 2) was performed in the MathCad environment. The results are shown in Table 1.

Table 1

Blade construction parameters

Inlet diameter D_0, mm	Impeller channel width at inlet b_1, mm	Impeller channel width at outlet b_2, mm	Impeller diameter D_2, mm	Number of blades Z	Specific speed n_s	Impeller efficiency (indicative)
26	31.75	12.75	128	6	47.62	0.8

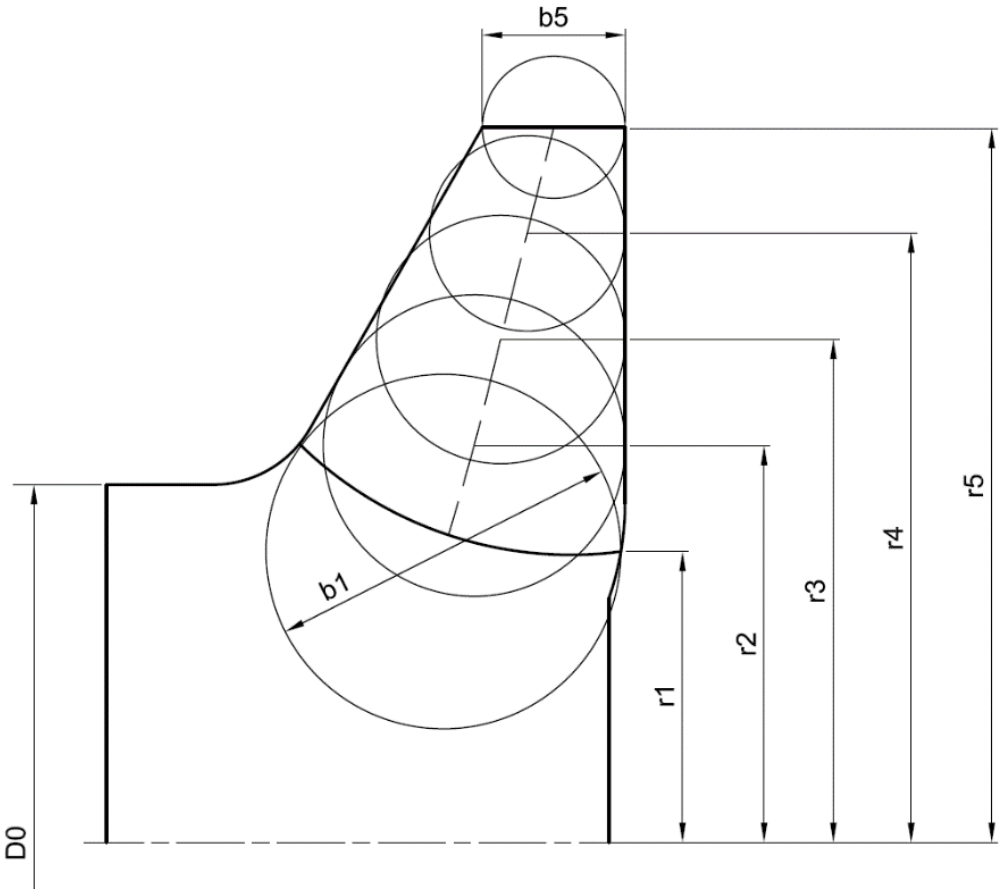

Figure 2. Modelling of the meridian section of pump impeller.

The differential equation of the blade profile in the plane is [10,11,18]:

$$r \cdot d\theta = \frac{dr}{tg\beta}. \tag{21}$$

From relation (21), we obtain the angle of deployment of the blade [10,11,18]:

$$\theta = \frac{180}{\pi}\int_{r_1}^{r_2}\frac{dr}{rtg\beta}. \tag{22}$$

The blade angle at any point surveyed at radius *r* can be determined if the distribution of relative velocity *w* and meridional velocity is known $a`_m$ without considering the compression along the radius and the thickness of the blade *S* along the length of the radius:

$$sin\beta = \frac{S}{t} + \frac{a`_m}{\omega}. \tag{23}$$

When integrating the relation (22) we obtain:

$$B(r) = \frac{1}{rtg\beta}. \tag{24}$$

At the end of the blade profiling, calculate, for any radius r_K, the wrap angle [10,11,18]:

$$\theta_K = \frac{180}{\pi}\sum_{i=1}^{K}\frac{B_1+B_{i+1}}{2}\Delta r_i. \quad (25)$$

The determination of the palette parameters was also carried out according to the methodology performed in [10] and is shown in Table 2.

Table 2

Blade construction parameters

Pos.	Radial coordinate r_k, mm	Impeller channel width b, mm	Axial velocity v'_m, m/s	Relative speed w, m/s	Pitch t, mm	Blade thickness δ, mm	Plate angle β°	Deployment angle θ°
1	26	31.75	2.58	11.95	27.21	2.50	17.92	0
2	35.5	27	2.99	11.68	37.16	3.00	19.70	27.51
3	45	22.25	3.13	11.41	47.10	3.50	20.40	48.37
4	54.5	17.5	2.98	11.14	57.04	3.25	18.94	65.15
5	64	12.75	2.55	10.86	66.99	3.00	16.23	79.15

4. Determination of impeller parameters obtained in ANSYS Workbench

4.1. Forming the geometric model in ANSYS DesignModeler

The geometric module used in the study was obtained in ANSYS DesignModeler. The ANSYS BladeEditor tool was applied to obtain the parameterized geometric model, Figure 3.

The blade geometry was parameterized by varying the angle β of the blade at 5 points, keeping the blade thickness distribution constant along the length of the blade. The values of angle β were recalculated considering the direction of the pump's impeller rotation and entered as input parameters in the DesignModeler environment, Figure 4.

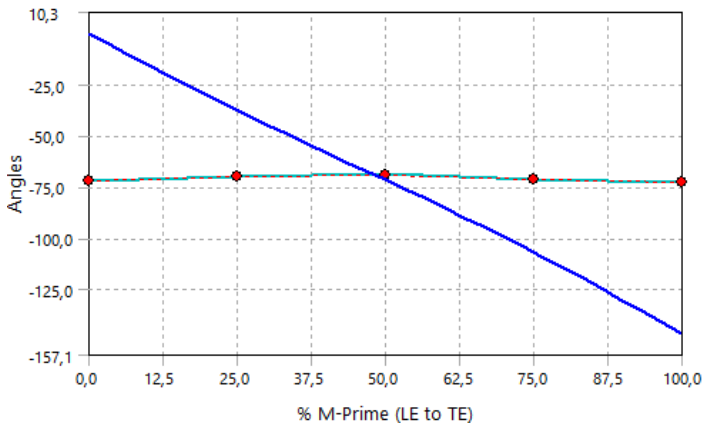

Figure 3. Distribution of geometrical parameters angle ϑ (blue) and θ (grey) in relation to the length l of the blade.

Figure 4. Geometry of the pump impeller blades obtained in ANSYS DM.

Comparing the geometry of the impeller obtained from analytical methods based on empirical models (Figure 4) with the original (Figure 5a) and the optimized (Figure 5b), we can see that the impeller has kept the same number of blades as the original one (Z = 6), but the blade wrap angle θ has been increased.

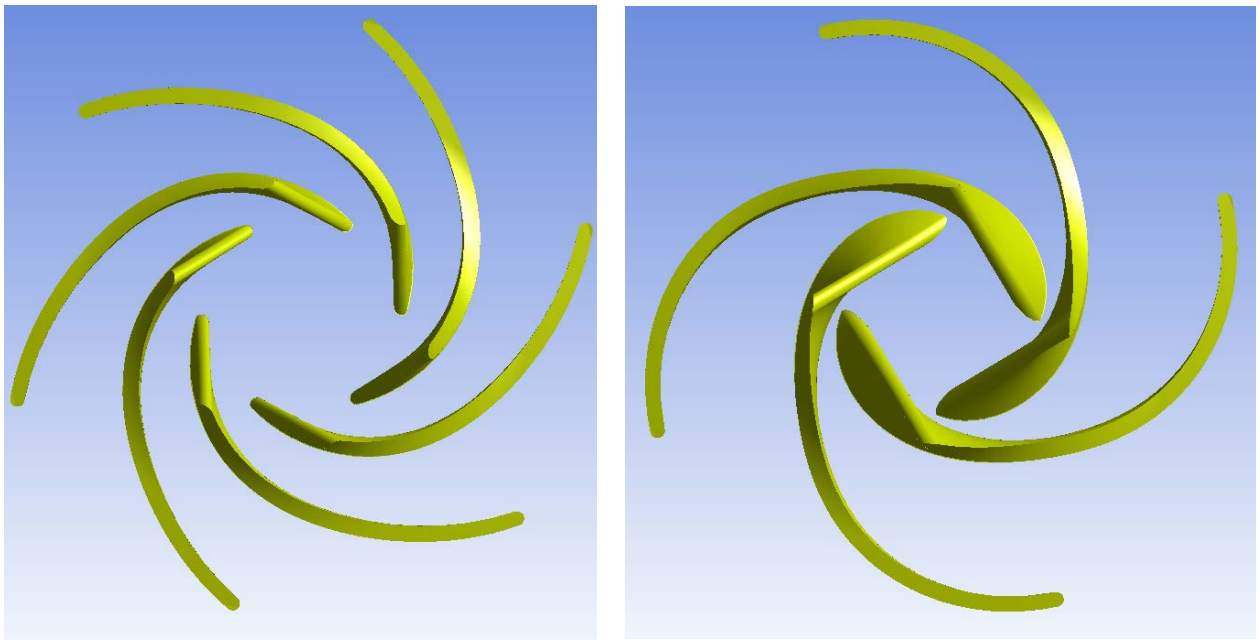

a) b)

Figure 5. Geometric model of the impellers:
a) the original impeller; b) the impeller with optimized blades

4.2. Forming the geometric model in ANSYS DesignModeler

Discretization of the pump impeller model was performed in ANSYS TurboGrid. This grid generator was chosen because it provides automated discretization [20] algorithms that can generate discretization grids for complex turbomachinery impeller geometries [21].

Figure 6 shows a grid created in ANSYS TurboGrid. The desired y^+ parameter equals to 1 and the Reynolds number of the fluid flow equals to $5 \cdot 10^5$ in the pump impeller. These settings were used to set the boundary layer's characteristics automatically. The application of ANSYS TurboGrid with the given parameters allows to obtain a sufficiently dense structured grid, including the boundary layer description, which is necessary for a proper description of the fluid flow. The discretization grid of the pump impeller obtained with $N_{R1} = 3 \cdot 10^6$ finite elements was obtained.

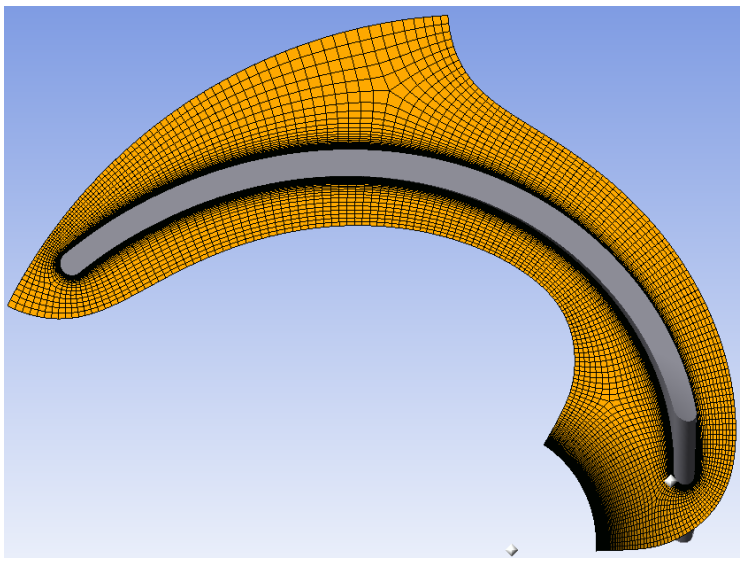

Figure 6. Structured discretization network obtained in ANSYS TurboGrid.

The ANSYS Meshing, a universal discretization environment, which thanks to its ease of representation is the most commonly applied grid generator used in ANSYS [21]. It was used to obtain the discretization grid of the suction connection and the pump casing volute.

In conducting the studies, the optimal discretization grid parameters were obtained in convergence studies from [21,22]. On the walls of the flow zone the finite element size of ΔS = 2 mm was selected, the inflation method with 20 inflation layers and the inflation layer thickness of 3 mm was applied. Also, in the case of the pump casing volute model on the area where the inflation method was applied, the sizing procedure with the finite element size of 1.25 mm was also applied. The discretization grid of the suction connection with $N_{S1} = 0.65 \cdot 10^6$ finite elements and the grid of the pump casing volute with $N_{S2} = 2.03 \cdot 10^6$ finite elements was obtained.

4.3. Flow simulation settings used in the study

The *Total Pressure* (P_{inlet} = 1MPa) is indicated at the pump **Inlet**, with a low turbulence state (1%). At the pump inlet the flow is completely formed of water in liquid form. The flow is considered isothermal (t = 25˚C), with zero reference pressure (P_{ref} = 0 atm).

At the **Outlet** of the pump casing discharge pipe, the *Bulk Mass Flow Rate*, (Q = 1.75 kg/s) is indicated. The flow characteristics related to turbulence and cavitation at the pump outlet are calculated with the Zero Gradient condition.

The impeller domain is required to run at 2950 min^{-1}. The SST (Shear Stress Transport) model [23] is used in the simulation to describe the turbulent flow, model being universal [21,24], which requires limited computational resources compared to transient models. Considering that the simulation is based on the two-phase continuous fluid model, the fluid consists of: *water in liquid form with a temperature of 25˚C and water vapors*. In the initial state the fluid consists of water in liquid form.

As a mass transfer model, the Zwart - Gerber - Belamri model [25] is applied. The following calculation characteristics were applied: vapor saturation pressure – 3170 Pa and mean bubble diameter – $2 \cdot 10^{-6}$.

As a *Timescale Control* model, the *Physical Timescale* option was selected, with time step equal to $1/\omega$ = 0.003237s.

4.4. Setting processing parameters

As a stop computation condition the following was selected: either the final number of 1000 computation iterations or the condition when the residual error tolerance of 10^{-5} was reached during the simulations. In order to monitor the convergence, the following indicators were selected: static and absolute pressure at inlet and outlet, as well as torque with respect to the rotation axis applied to the pump impeller. From Figure 7 we can see that the calculation is convergent.

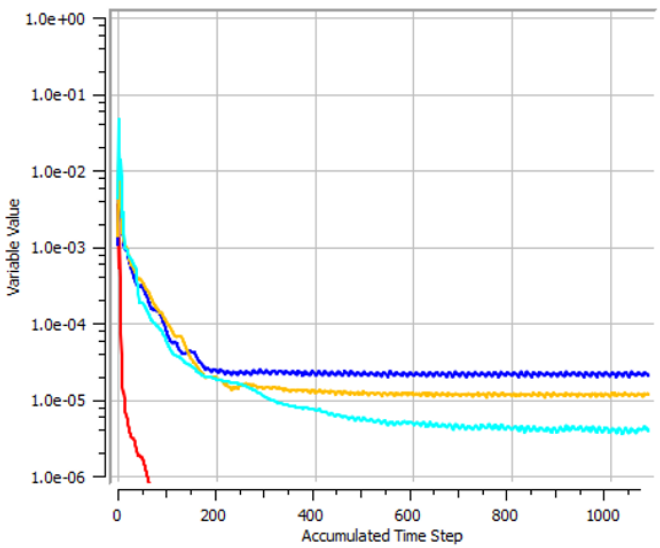

Figure 7. Root mean square errors.

4.5. Analysis of the obtained results

The simulation of the pump's impeller flow zone was performed. The simulation results are shown in Figure 8.

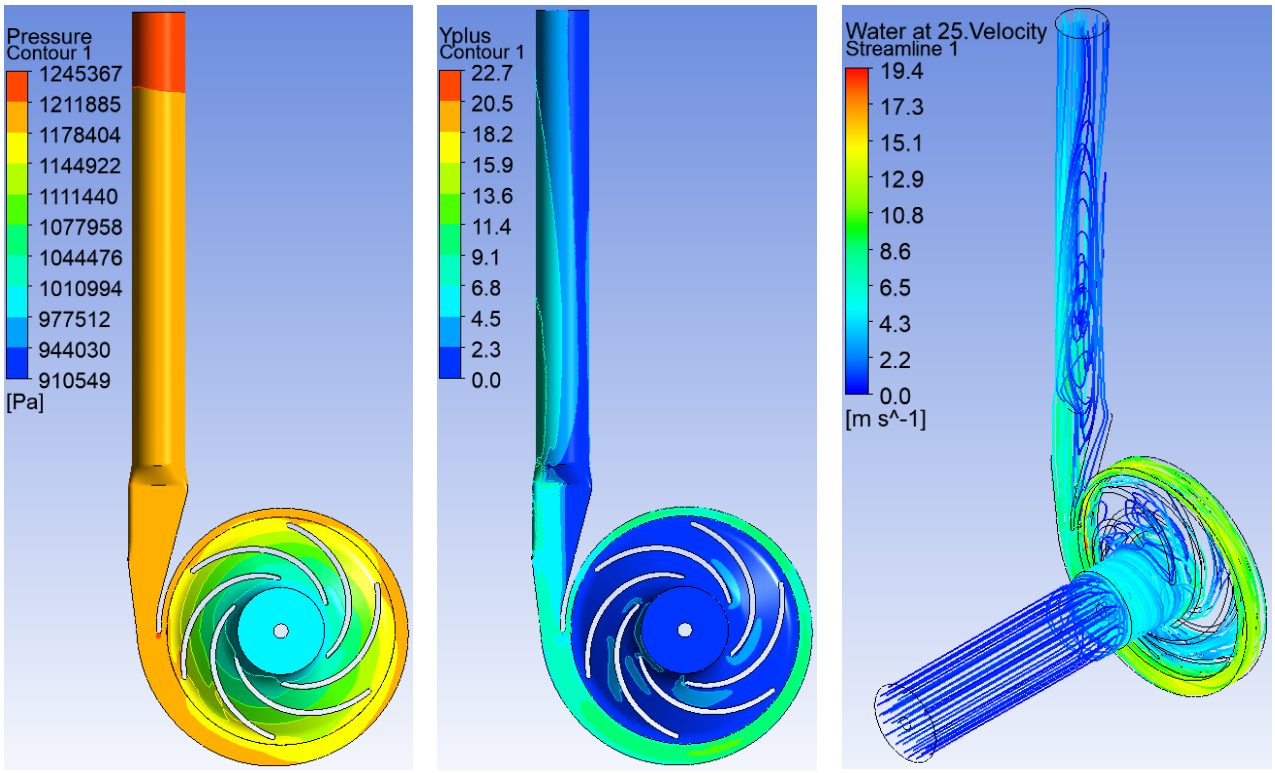

a) b) c)

Figure 8. Flow simulation results in the flow zone of the pump with impeller obtained by analytical calculation: a) pressure field distribution; b) y^+ parameter values distribution; c) streamlines showing flow velocity.

The comparison of the characteristics of the pump with impeller geometrical parameters obtained by analytical calculations, with original one and with optimized impeller obtained by coupling CFD calculations and optimization algorithms are shown in Table 3.

Table 3

Comparison of the pump's impeller characteristics

Impeller geometry	Pumping load, mH_2O	Torque, Nm	Impeller efficiency	Pump efficiency
Original	20.8	2.03	0.56	0.363
With optimized blades	19.9	1.776	0.619	0.396
Analytically calculated	21	1.91	0.6	0.384

The highest efficiency was obtained by the impeller with optimized blades η_{rot}= 61.9%, but the impeller obtained by analytical calculations η_{rot} = 60%, also shows superior characteristics to the original one. We can also see that the analytically calculated impeller presented the highest pumping head of all the presented impellers, but within the allowed limits.

5. Conclusions

The theoretical considerations on centrifugal pumps have been presented in the paper. We can see that, although over the years we can notice a significant progress in theory, the empirical computational models are losing to optimizations based on CFD simulations and optimization algorithms, but can be used as a benchmark in an optimization process.

The calculation based on the empirical model of the geometrical parameters of the centrifugal pump impeller was carried out and compared with the optimized geometrical model. We can see that the highest efficiency was obtained by the impeller with optimized blades η_{rot} = 61.9%, but the impeller obtained by analytical calculations η_{rot} = 60%, which is higher compared to the original impeller η_{rot} = 56%.

Conflicts of interest: The authors declare no conflict of interest.

References

1. Sudadiyo, S. Preliminary design of RDE feedwater pump impeller. *Tri Dasa Mega* 2018, 20, 1, doi:10.17146/tdm.2018.20.1.3647.
2. Djodikusumo, I.; Diasta, I.N.; Sanjaya Awaluddin, I. Geometric Modeling of a Propeller Turbine Runner Using ANSYS BladeGen, Meshing Using ANSYS TurboGrid and Fluid Dynamic Simulation Using ANSYS Fluent. *AMM* 2016, 842, 164–177. doi:10.4028/www.scientific.net/AMM.842.164.
3. Yang, L.F.; Zhang, S.R.; Liu, W.N.; Yang, Y.; Zhang, Y.J. Application ANSYS CFX in Modeling Turbine Blade. *MSF* 2009, 626–627, pp. 593–598. doi:10.4028/www.scientific.net/MSF.626-627.593.
4. Checcucci, M.; Sazzini, F.; Marconcini, M.; Arnone, A.; Coneri, M.; De Franco, L.; Toselli, M. Assessment of a Neural-Network-Based Optimization Tool: A Low Specific-Speed Impeller Application. *International Journal of Rotating Machinery* 2011, pp. 1–11, doi:10.1155/2011/817547.
5. Derakhshan, S.; Bashiri, M. Investigation of an Efficient Shape Optimization Procedure for Centrifugal Pump Impeller Using Eagle Strategy Algorithm and ANN (Case Study: Slurry Flow). *Struct Multidisc Optim* 2018, 58, 459–473, doi:10.1007/s00158-018-1897-3.
6. Kim, B.; Siddique, M.H.; Samad, A.; Lee, D. E. Optimization of Centrifugal Pump Impeller for Pumping Viscous Fluids Using Direct Design Optimization Technique. *Machines* 2022, 10, 774, doi:10.3390/machines10090774.
7. Zhang, Y.; Hu, S.; Wu, J.; Zhang, Y.; Chen, L. Multi-Objective Optimization of Double Suction Centrifugal Pump Using Kriging Metamodels. *Advances in Engineering Software* 2014, 74, pp. 16–26, doi:10.1016/j.advengsoft.2014.04.001.
8. Gülich, J.F. *Centrifugal Pumps*. Springer International Publishing, Cham, 2020, 1264 p.
9. Bostan, V.; Petco, A. Minimizing Blade-Fluid Energy Losses in Centrifugal Hydraulic Pump Impellers. *Proceedings of the Acta Technica Napocensis* 2023, 67(4).
10. Lomakin A.A. *Centrobezhnye i osevye nasosy*. Mashinostroenie, Moskva, 1966, 363 p. [In Russian].
11. Mihajlov, A.K.; Malyushenko, V.V. *Lopastnye nasosy. Teoriya, raschet I konstruirovanie*. Mashinostroenie, Moskva, 1977, 288 p. [in Russian].
12. *Centrifugal Pump Handbook*. Sulzer Pumps Ltd, Ed.; 3. ed., repr.; Elsevier Butterworth-Heinemann: Amsterdam Heidelberg, 2011, 289 p. ISBN 978-0-7506-8612-9.
13. Miloş, T. *Pompe şi ventilatoare centrifuge şi axiale*. Politehnica, Timişoara, 2009, 268 p.
14. Anton, L.E.; Baya, A.; Milos, T.; Stuparu, A. *Hidrodinamică experimentală*. Orizonturi Universitare, Timişoara, 2007, 360p. ISBN 978-973-638-330-4.
15. Dick, E. Fundamentals of Turbomachines. Springer International Publishing, Cham, 2022, 564 p.
16. Ciobanu, B. *Turbomaşini hidraulice. Partea I – Turbogeneratoare*. Tehnopress, Iași, Romania, 2008, 206 p.
17. Bashta, T.M.; Rudnev, S.S.; Nekrasov, B.B. *Gidravlika, gidromashiny i gidroprivody*. Al'yans, Moskva, 2010, 423 p. [in Russian].
18. Ivanovskij, V.N.; Sabirov, A.A.; Degovcov, A.V.; Pekin, S.S.; Donskoj, YU.A. *Proektirovanie i Issledovanie Stupenej Dinamicheskih Nasosov*. IC RGU nefti i gaza, Moskva, 2015, 124 p. [in Russian].
19. Arinushkin, L.S.; Abramovich, R.B.; Polinovskij, A.Yu.; Leshchiner, L.B.; Glozman, E.A. *Aviacionnye centrobezhnye nasosnye agregaty*. Mashinostroenie, Moskva, 1967, 255 p.

20. Ansys TurboGrid User's Guide. Release 2021 R2. Available online: www.ansys.com (accessed on 18 September 2023).
21. Bostan, V.; Petco, A. Determining Optimal Simulation Settings for the Centrifugal Pump Parts Optimization Process. *Journal of Engineering Science* 2023, 30(2), pp. 8–22. doi.org/10.52326/jes.utm.2023.30(2).01.
22. Petco, A. Numerical simulation of liquid flow in centrifugal pump working parts using Ansys CFX. In: Technical-scientific conference of students, masters and PhD students, TUM, Chisinau, 2021, 1, pp. 504–507.
23. Menter, F.R. Two-Equation Eddy-Viscosity Turbulence Models for Engineering Applications. *AIAA Journal* 1994, 32, pp. 1598–1605.
24. Menter, F.R.; Sechner, R.; Matyushenko, A. Best Practice: RANS Turbulence Modeling in Ansys CFD. Available online: www.ansys.com (accessed on 18 September 2023).
25. Zwart, P.; Gerber, A.G.; Belamri, T. A Two-Phase Flow Model for Predicting Cavitation Dynamics. In: *Fifth International Conference on Multiphase Flow* 2004.

Citation: Bostan, V.; Petco, A.; Șaragov, I. Empirical models' applicability for calculating the centrifugal pump's impellers geometric parameters. *Journal of Engineering Science* 2023, 30 (4), pp. 8-19. https://doi.org/10.52326/jes.utm.2023.30(4).01.

Submission of manuscripts: jes@meridian.utm.md